Journal of Civil Engineering and Management
ISSN 1392-3730 / eISSN 1822-3605
2020 Volume 26 Issue 3: 227–246
https://doi.org/10.3846/jcem.2020.12181

PERFORMANCE STUDY OF SC WALL BASED ON EXPERIMENT AND PARAMETRIC ANALYSIS

Qi GE[1], Tao HE[2], Feng XIONG[1*], Peng ZHAO[1], Yang LU[1], Yang LIU[1], Ning ZHOU[3]

[1]*MOE Key Laboratory of Deep Underground Science and Engineering, School of Architecture and Environment, Sichuan University, 610065 Chengdu, China*
[2]*Poly (Chengdu) Industrial Co., LTD, Chengdu, China*
[3]*The Eleventh Design & Research Institute of IT Co., Ltd., Chengdu, China*

Received 30 May 2019; accepted 04 November 2019

Abstract. Reverse cyclic lateral testing was undertaken to investigate the seismic behavior of 1/4 scale steel-plate concrete (SC) composite walls. The experimental program involved seven SC wall pier specimens. A new chamber structure is proposed, using steel diaphragms to connect the two steel faceplates to each other and to divide the SC wall pier into two parts. Conventional wall specimens failed mainly by tensile fracture of the concrete at the junction of the wall side and wall base, crushing of the concrete at the toe of the wall, or buckling of the steel faceplate. Tearing of the welded joints at the steel faceplates and steel diaphragm, buckling of steel, steel diaphragms being pulled out, tensile fracture and crushing of the concrete were the main failure modes of the chamber structure walls. A parametric numerical analysis in ABAQUS was developed to investigate the effects of the stiffening rib, steel web amount, material strength, shear-span ratio, and axial compression ratio on the seismic response of SC walls. The chamber structure of the SC wall piers can improve the peak load, ductility, and energy-dissipating capacity. The steel faceplate thickness and stiffening ribs can improve the behavior of SC wall piers.

Keywords: steel-plate concrete, composite wall, cyclic lateral loading, chamber structure wall, parametric analysis, performance study.

Introduction

Reactor containment structures for reactor-cavities in nuclear power plants have a variety of forms, including steel structures, reinforced concrete walls, prestressed reinforced concrete walls and other composite structures. Steel-plate concrete (SC) composite walls, as a new type of composite structure, have been applied to reactor containment structures and shielding buildings in nuclear power plants in recent decades (DCD, 2011, 2012), and have gained popularity, especially after the earthquake that occurred in northeastern Japan on March 11, 2011. SC walls, which have a lateral force resisting system typically comprised of thick infilled concrete, two exterior steel faceplates, headed steel studs attaching the steel faceplates to the concrete core, and tie rods or steel diaphragms joining the steel faceplates to each other, have many advantages over conventional reinforced concrete shear walls. These advantages include higher strength and ductility due to the composite effect of the steel plates and the infilled concrete (Takeuchi et al., 1998; Bruhl et al., 2015a), reduced thickness and weight, convenient and shorter construction time (Schlaseman, 2004), lower cost, and reduced seismic force demands under membrane forces and out-of-plane moments (Varma et al., 2014).

Research on SC walls initially started in Japan in the 1980s (Fukumoto et al., 1987). Over the past thirty years, extensive research and development work on the design, analysis, testing and mechanical behavior of SC walls on the basis of previous research has been done in China, the United States, South Korea, the United Kingdom and Japan (Huang & Liew, 2016; Ji et al., 2013; Link & Elwi, 1995; Kim et al., 2009; Oduyemi & Wright, 1989; Ozaki et al., 2004). SC wall experiments have focused on in-plane shear loading (Anwar & Wright, 2004; Ozaki et al., 2004; Eom et al., 2009; Epackachi et al., 2013, 2015a; Varma et al., 2014; Kurt et al., 2016; Seo et al., 2016), out-of-plane shear loading (Hong et al., 2010; Sener et al., 2013; Sener

*Corresponding author. E-mail: *fxiong@scu.edu.cn*

& Varma, 2014; Varma et al., 2014), axial compression loading (Fukumoto et al., 1987; Usami et al., 1995; Takeuchi et al., 1998; Wright, 1998; Choi & Han, 2009; Zhang et al., 2014; Huang & Liew, 2016), impact loading (Remennikov et al., 2013; Sohel & Liew, 2014; Zhao & Guo, 2018), and analysis and design for combined thermal and mechanical loading (Booth et al., 2007; Varma et al., 2009, 2011a; Eom et al., 2009; Epackachi et al., 2013, 2015a), and Kurt et al. (2016) tested SC walls under cyclic lateral loading to investigate the load-carrying capacity, ductility, and the effects of varying wall type, wall thickness, cross-sectional shape, reinforcement ratio, stud spacing, tie bar spacing, and strengthening methods at the wall base on the shearing response. The studies in Eom et al. (2009) showed that the faceplates prevented early fracture of the steel plate welded at the wall base and improved the shear response of the wall. It was also indicated that SC walls failed due to buckling of the steel plate and crushing of the infilled concrete, and the different strengthening methods used for the wall base significantly affected the ductility of the walls. Epackachi et al. (2013, 2015a) focused on the inelastic range of responses to investigate the response of SC walls under cyclic lateral loading, in which the walls were anchored to a concrete basement with a pre-tensioned bolted connection that was designed to be stronger than the walls. The results showed that the post-peak load behavior of the walls was influenced by the faceplate slenderness ratio, with a smaller rate of post peak load degradation observed in the wall with the smallest faceplate slenderness ratio. The results also indicated that the distance between the baseplate and the first row of connectors affected the post peak shear strength behavior and the subsequent fracture of the faceplates. Moreover, the connection of the SC wall to the foundation block had a significant influence on the initial stiffness of the walls. Kurt et al. (2016) studied the seismic behavior and ductility of SC wall piers without boundary elements, which showed that SC wall piers with aspect ratios greater than or equal to 0.60 failed because of in-plane bending or flexure. The behavior and failure was governed by cyclic yielding and local buckling of the steel faceplates, concrete crushing, and eventually steel tension fracture. The lateral load capacity of the SC wall piers was governed by the in-plane flexural capacity of the wall cross section at the base. Ju and Zeng (2015) investigated the uplift performance of stud connectors in SC structures by testing and numerical methods. The results showed that the static ultimate bearing capacity, under which the stud connector was pulled out from the damaged reinforced concrete, was much larger than the cyclic ultimate bearing capacity, at which the weld joint between stud and steel plate fractured.

Hong et al. (2010) proposed shear-strength-models based on plasticity theory limit analysis and verified these models with experimental results to investigate the out-of-plane shear behavior of SC walls, which are similar to reinforced concrete (RC) walls, conducting beam tests in one-way bending. The out-of-plane shear strengths from SC beams provided by Chinese, Japanese, South Korean, and US researchers were summarized and compared with shear strength calculations based on the design codes in Japan for SC – JEAC 4618 (Japanese Electric Association Nuclear Standards Committee, 2009), South Korea for SC – KEPIC SNG (Board of KEPIC Policy Structural Committee, 2010) and the US for RC (ACI 349 Committee, 2006) (Sener et al., 2013; Sener & Varma, 2014). The results showed that the ACI 318 code (American Concrete Institute [ACI], 2014) equations reasonably estimated the lower bound out-of-plane shear strength of SC walls with larger shear span-to-depth ratios and section depth; however, the Japanese and South Korean code equations gave overestimations. Kim and Choi (2011) studied the shear strength of the connections between open and closed SC structures, which showed that the shear resistance at the interface was enhanced by the shear capacity of the shear plate as well as the friction caused by the compressive force along the wall plate. Usami et al. (1995) and Takeuchi et al. (1998) conducted experiments to investigate the buckling characteristics of steel faceplates under compression loading. Their studies indicated that the buckling and yielding of the steel plate did not abruptly affect the overall axial load displacement relationship of the SC walls. Euler's equation for the elastic buckling of columns with one fixed end and one pin-jointed end can be used to evaluate the buckling stress of the steel plate. Zhang et al. (2014) studied the effects of shear connector design on the level of composite action and the development length of steel faceplates in SC walls. The result showed that adequate (75–90%) partial composite action develops in SC walls with lower reinforcement ratio and with smaller stud spacing (lower s/tp ratios). So using more shear studs to increase the partial composite action can be structurally and economically inefficient. Choi et al. (2013) studied the buckling patterns and determined the squash load of (SC) walls by varying the width-thickness ratio and yield strength of the surface steel plates by testing six SC walls.

Full scale tests by Wright (1998), when subjected to axial loading, showed that the local buckling of the steel faceplate and the profile shape of the cross-section had influence on the axial loading capacity. SC walls were subjected to thermal and mechanical loading by Booth et al. (2007) and Varma et al. (2011a) for the purpose of studying the effect of thermal loading on the shear and flexural responses. The results indicated that cracked transformed section properties could be used to reasonably predict the out-of-plane flexural stiffness of SC walls away from the heated region. The concrete cracking occurred in the center of the heated region because of the thermal gradient through the SC wall depth. Booth et al. (2015) also studied the out-of-plane flexural response of SC walls subjected to accidental thermal and mechanical loading in four full-scale beam tests, which showed that thermal loads reduce the out-of-plane flexural stiffness of SC walls. Large scale experiments referring to inelastic behavior are very important for fully studying the shear response of SC walls for use in civil engineering and safety-related nuclear structures.

Some relevant numerical studies have been performed during the past twenty years (Braverman et al., 1997; Emori, 2002; Varma et al., 2011b; Kurt et al., 2013, 2016; Epackachi et al. 2015a; Sener et al., 2015, 2016; Booth et al., 2015; Bruhl et al., 2015b). Braverman et al. (1997) used ANSYS to develop a model to simulate the behavior of SC walls under monotonically loading, in which a bilinear stress-strain curve and a linear elastic-perfectly plastic model were applied to represent the uniaxial behavior of the steel faceplates and the compressive stress-strain relationship of the infilled concrete, respectively. This model assumed that the analysis was stopped when the peak strength of the SC walls was reached. The results indicated that the initial stiffness and peak compressive force attained by the model were in good agreement with the experimental results. Bruhl et al. (2015a) developed 3D finite element models to predict the behavior and local failure of SC walls subjected to missile impact using LS-DYNA. Other researchers also conducted finite element (FE) modelling of SC walls for calculating in-plane and out-of-plane shear responses in LS-DYNA (Kurt et al., 2016; Epackachi, 2014; Epackachi et al., 2015b, 2015c). Kurt et al. (2016) performed a parametric study of SC walls to investigate the effect of aspect ratio, thickness, and reinforcement ratio on the lateral load capacity of SC walls piers using LS-DYNA models. The parametric study showed that the lateral load capacity of SC wall piers increased as the wall aspect ratio decreased, but never reached the in-plane shear strength of the steel faceplates alone. As the wall aspect ratio exceeded 1.5, the lateral load capacity of SC wall piers was governed by the plastic moment capacity of the SC wall cross section at the base. Epackachi (2014) conducted FE modeling in LS-DYNA to obtain a well-predicted response to the peak shear force but underestimated the post-peak responses, in which a perfect bond between the steel faceplates and the infilled concrete was assumed. This research was continued by Epackachi et al. (2015b, 2015c) and focused on both the pre- and post-peak responses of SC walls, considering the friction between steel faceplates and the infilled concrete, buckling of the steel faceplates, and foundation flexibility. ABAQUS was also used to develop models to simulate the out-of-plane and in-plane shear behavior of SC walls (Chaudhary et al., 2011; Varma et al., 2011b; Varma & Sener, 2013; Ali et al., 2013; Nguyen & Whittaker, 2017). Reinforcement ratio, connector type, and faceplate slenderness ratio were the key design variables to study the effect of the variables on the performance of SC walls (Nguyen & Whittaker, 2017). The result showed that the steel faceplates contribute between 20% and 70% of the total shearing resistance of the SC wall piers evaluated, depending on the reinforcement ratio, faceplate slenderness ratio, story drift, and level of damage.

SC walls using intersecting cross walls as boundary elements or flanges are being used in safety-related nuclear facilities as part of containment internal structures, and the in-plane shear resistance of walls and the overturning moment resistance of the flange walls are crucial to the lateral load behavior of these structures. Most prior research has thus focused on the in-plane shear behavior and strength of SC walls (Seo et al., 2016). Some authors recently studied SC walls without boundary elements or flanges (Kurt et al., 2016; Epackachi et al., 2015a), where the lateral load behavior is very different from the in-plane shear behavior of SC walls with boundary elements or flanges. Both the overturning moment and the shear force at the base are very important to the in-plane behavior of SC walls without boundary elements or flanges. This difference was discussed in Kurt et al. (2016). In the future, SC walls without boundary elements may be widely used in commercial building construction.

This paper addresses the in-plane behavior of SC walls without boundary elements. The research results provide certain reference values for SC wall piers without boundary elements, which may be used in structures in the future. In the present study, the inelastic cyclic lateral load response of four SC wall pier specimens was addressed under in-plane loading. A new chamber structure, with steel diaphragms joining the two steel faceplates, is also presented. The effects of the stiffening rib, steel web, varying steel faceplate thickness on the seismic response of SC walls were evaluated in experimental and parametric studies. The following sections describe the experimental program, testing phenomenon, and key experimental and parametric results.

1. Experimental program

The prototype, the SC wall, is used as a shield structure for the reactor-cavity in a Chinese API1000 nuclear power plant. The shield structure is a cylindrical structure and an airtight construction to prevent the leakage in the nuclear power plant. According to the parameters of the prototype SC wall, four 1/4 scale specimens of SC wall piers subjected to cyclic lateral loading were designed and tested. The parameters of the prototype specimen and test specimen are shown in Table 1. The design details and dimension parameters of the test specimens are shown in Table 2. When purchasing test materials, the steel plate manufacturer produces the steel plate with the particular modulus and a certain size. When we bought the steel plate from this factory, and the actual thicknesses of the steel plate at that time were 2.75 mm and 3.75 mm, but not 3 mm and 4 mm, respectively. So the thicknesses of the steel plates that were available were 2.75 mm and 3.75 mm, so the actual thicknesses of the steel plates were 2.75 mm and 3.75 mm. The elastic modulus, density, yield strength and ultimate strength of the steel plate were 2.06×10^5 MPa, 7850 kg/m^3, 255 MPa and 395 MPa, respectively. The SC wall pier test setup and side view are shown in Figure 1. The tie rod in the paper was used as a testing measure to make sure the infilled concrete had sufficient thickness during concrete pouring. It was not a part of the SC wall piers for improving the strength in the plane. After concrete pouring, the tie rod could not be removed, and the effect on the SC wall piers was ignored because spot welding was used. The test parameters were the faceplate thickness, stiffening rib, and steel diaphragm.

Table 1. Parameters of the prototype specimen and test specimen

Specimen type	Wall thickness (mm)	Steel thickness (mm)	Concrete thickness (mm)	Stud (mm)	Steel material	Concrete Compression Strength (MPa)
Prototype	900	12	876	Φ20×150@250	ASTM A36	27.6
Test	225	3	219	Φ6×40@60(120)	Q235	27.5(C60)

Table 2. Test specimen details

Specimen	Wall dimension (L×T×H)(mm)	Faceplate thickness, T_f (mm)	Stud	Stiffening rib	Steel diaphragm	Reinforcement ratio $2T_f/T$(%)	Slenderness ratio
SCWA-1	800×225×1420	2.75	Φ6×40@75	60×3@150	–	2.44%	27
SCWA-2	800×225×1420	3.75	Φ6×40@75	60×3@150	–	3.33%	20
SCWB-1	800×225×1420	2.75	Φ6×40@75	–	3 mm@400	2.44%	27
SCWB-2	800×225×1420	3.75	Φ6×40@75	–	3 mm@400	3.33%	20

a) SC wall piers test setup

b) SCWA wall pier side view

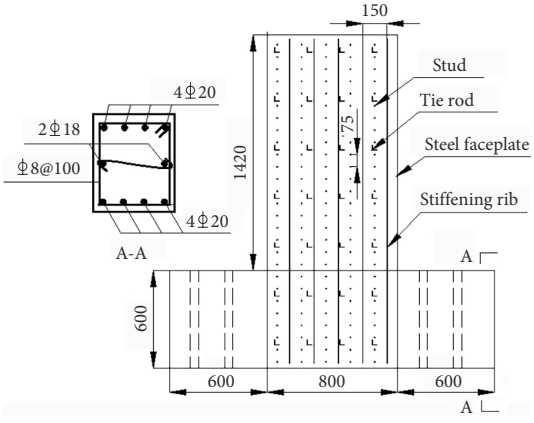

c) SCWB wall pier side view

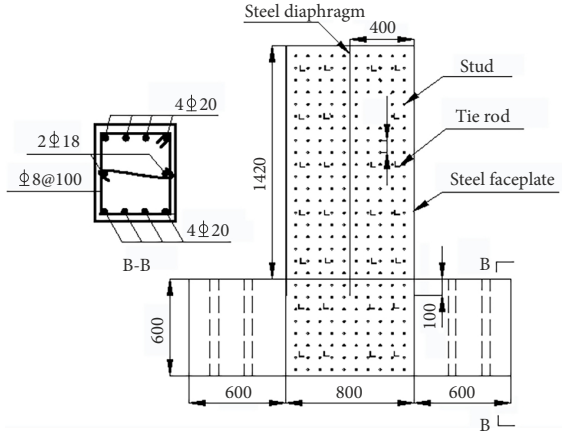

Figure 1. Overview of SC wall pier. All units are given in mm

1.1. Test specimen description for specimens SCWA and SCWB

Prior research showed that the ductility of the SC wall piers was significantly influenced by the strengthening methods used for the wall base (Eom et al., 2009). In order to prevent the foundation from being damaged first and the steel faceplates being pulled out from the foundation before SC wall piers reach to the ultimate bearing capacity, the foundations of the specimens SCWA and SCWB were strengthened. The wall bases were reinforced concrete structures. For specimens SCWA-1, SCWA-2, SCWB-1, and SCWB-2, the base size was 500×600×2000 mm. A steel plate of thickness 14 mm was embedded at the

bottom of the wall base, and a steel faceplate was inserted and welded to the steel plate. Steel studs on the steel plate at the bottom were also used to connect the steel plate to the concrete core, as shown in Figure 2. The steel plate was connected to the rigid base by threaded bars and the reserved holes.

SCWA and SCWB specimens had an H value of 1420 mm and the stud spacing of 75 mm, as shown in Table 2. The specimen group SCWA was designed by stiffening ribs, attaching faceplates to the infilled concrete, as shown in Figure 3(a), while the specimen group SCWB was a chamber structure with steel diaphragms joining the two faceplates to each other and dividing the SC wall piers into two parts, as shown in Figure 3(b). Different interior structures were designed in order to study the effect of interior structure type on the seismic performance of SC wall piers. According to the thickness of steel faceplates in the prototype SC wall, the thickness of the steel diaphragm was designed to be close to the thickness of the steel faceplates, 3 mm. The length of the wall was 800 mm, so it was appropriate that one steel diaphragm was arranged in the middle of the walls in SCWB. Two end plates were set at the two sides of the specimens SCWB-1 and SCWB-2 and attached to the steel faceplates. The differences between specimens SCWA-1 and SCWA-2, and between specimens SCWB-1 and SCWB-2 were only in the steel faceplate thicknesses of 2.75 mm and 3.75 mm, respectively, the purpose of which was to investigate the effect of the steel faceplate thickness on the performance of the SC wall piers in the same interior structure. The slenderness ratios of SCWA-1, SCWA-2, SCWB-1 and SCWB-2 were 20, 27, 20 and 27, respectively.

The connection between the stud and faceplate was manufactured first. The next stage was to weld the stiffening diaphragm and the angle steel. The other faceplate was then connected to the stiffening diaphragm and the angle steel. The two stiffening diaphragms at the side edges were welded to the two faceplates. The whole specimen was connected to the steel plate which was embedded at the bottom of the wall base. The final process was concrete pouring. Figures 4 to 6 show the welding details between steel diaphragm and faceplate and between stud and faceplate in the specimens SCWB-1 and SCWB-2. A

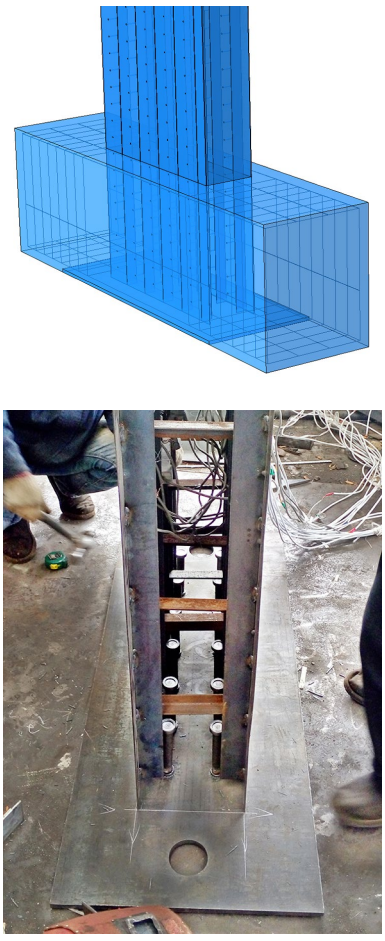

Figure 2. Connection between steel faceplate and wall base of SCWA and SCW

full welding method was used for the stud by a double-screw bolt welding machine, and porcelain protection was used to avoid severe heating deformation of the steel plate caused by temperature concentration, as shown in Figure 4. Manual Carbon dioxide shielded arc welding was applied in the other parts, as shown in Figures 5 and 6. The key point of precision assembling was the verticality of specimen. In the experiment, the tie rods were welded on the faceplate and not strongly welded using spot welding, as they did not bear the load of the specimen.

a) Specimen SCWA

b) Specimen SCWB

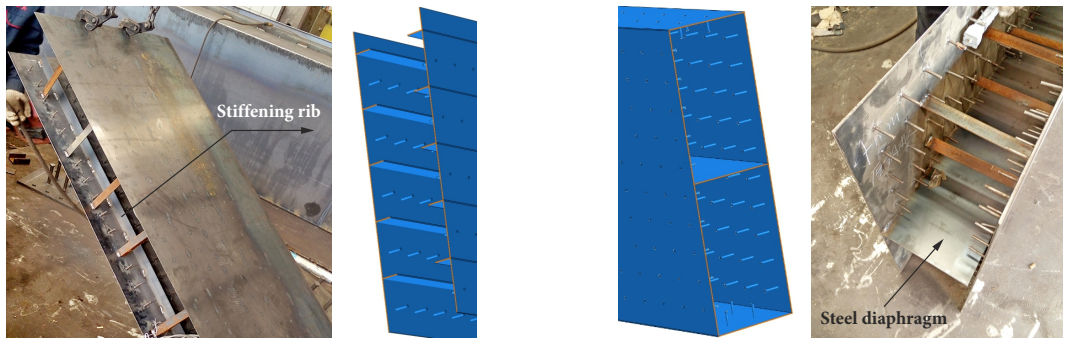

Figure 3. Difference between specimens SCWA and SCWB

Figure 4. Welding detail of stud

Figure 5. Connection details for steel diaphragm in SCWB-1 specmens

1.2. Instrumentation and loading

A 2,000-kN actuator was used to apply quasi-static cyclic lateral loads at the top of the wall specimens via loading brackets, in which two special loading steel beams were designed for the lateral and vertical loads, as shown in Figure 7. The steel beam for this steel roller support was placed at the bottom of the beam and oil was also daubed on the beam, in order to apply vertical loads (150 kN) and to allow the top of the SC wall piers to move freely in the horizontal direction, as shown in Figure 7. A customized steel beam was connected to the actuator for applying the lateral loads. A steel plate was welded to the top of the two steel faceplates and connected to the customized steel beam by threaded bars and reserved holes. Steel studs on the top steel plate were also used to connect the top steel plate to the concrete core, as shown in Figure 7(c). The steel beam connected the top steel plate to the actuator

Figure 6. Connection details for stiffening rib and steel diaphragm in SCWB-2 specmens

to provide the lateral force. The wall base was anchored to a strong floor with four 60-mm diameter high strength screws to prevent wall base movement during testing. The lateral load was applied at the top of the wall before the wall yielded, where the load differences were 20 kN and 40 kN at a speed of 2 kN/s for the initial loading and after the concrete cracking, respectively. When the first yield of the steel faceplates at the ends occurred, the SC walls yielded. Displacement-control was used after the wall yielded and the displacement difference in the two cycles of loading was equal to the yield displacement Δy at a speed of 0.1 mm/s. In each loading cycle, a push was applied first, followed by a pull, where the push and pull loadings were defined as positive and negative loads, respectively. The loading history is shown in Figure 8. The tests were terminated when either the walls were completely damaged or the specimens reached their ultimate bearing capacity. The ultimate bearing capacity is defined as that when the bearing capacity is less than 85% of the peak load after the loading reached the peak load of a particular specimen. Laser displacement transducers were located at the top and the bottom of the SC wall piers.

2. Experimental results

2.1. Testing phenomenon

Specimens SCWA-1 and SCWA-2 had similar failure progressions, including elastic deformation, flexural cracking of the infilled concrete, steel faceplate yielding, local buckling of the steel faceplate, crushing of the infill concrete, peak loading, spalling of the wall base concrete, and wall failure, are defined as follows: Elastic deformation occurs at the start of the test and continues until the first crack in the concrete is observed. Next, the concrete fracture stage

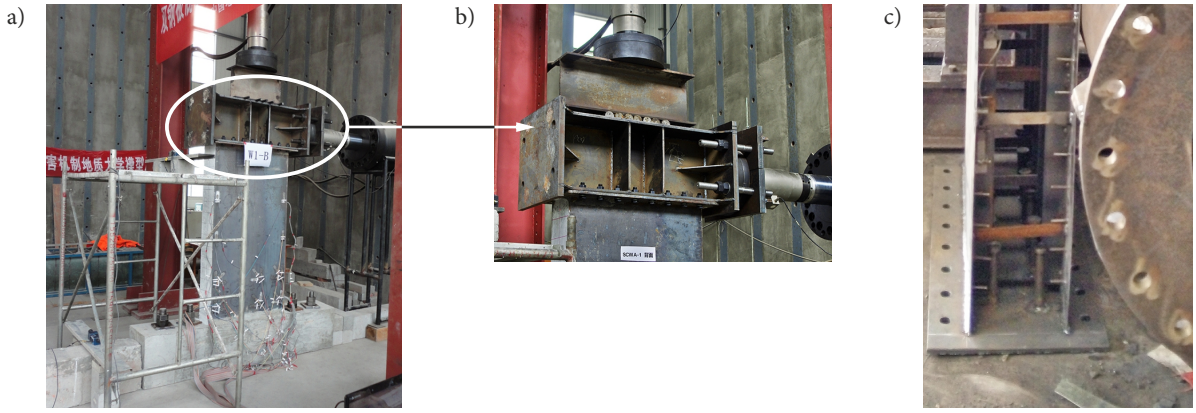

Figure 7. Test setup and loading steel beams

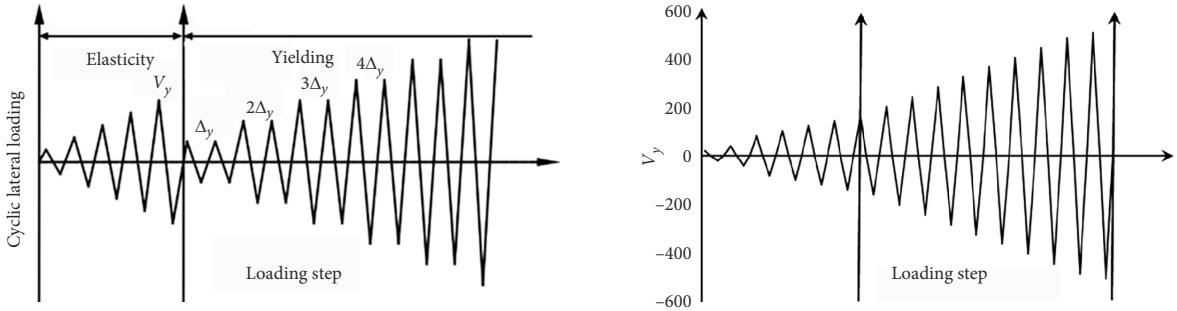

Figure 8. Loading history

follows until the steel starts to yield which leads to the steel faceplate yielding stage. As the lateral force increases, local buckling of the steel faceplates occurs. The infill concrete crushes with increasing loading and deformation. The specimen then enters the peak load stage where the loading reaches its peak. The wall base is not strong enough, so the wall base concrete spalls. Finally, the specimen, after being continuously loaded either experiences failure or a bearing capacity of less than 85%, whichever comes first. This is defined as the failure stage. Here, failure means that the SC wall cannot continue to bear loading because of the concrete damage and steel faceplate buckling.

However, specimen SCWB had a different progression: elastic deformation, pulling out of the steel diaphragm, faceplate yielding, peak load, and failure stages. The reasons behind the failure of SCWA and SCWB specimens were mainly due to the buckling of the steel faceplate and the tension and crushing of the wall concrete at the toe of the wall. Details of the observed behavior are presented in the following sections.

2.1.1. Flexural cracking of the infill concrete

All the SC wall piers underwent elastic deformation and no visible cracks occurred at a loading of 80 kN. At a loading of 100 kN, cracks in the concrete tension area for specimens SCWA-1 and SCWA-2 occurred in the plane of the wall, with widths of 0.2 mm and 0.1 mm, respectively, and distances of 240 mm and 200 mm from the wall base, respectively, as shown in Figures 9(a) and 9(b). Tiny cracks occurred at the junction of the wall side and wall base at loadings of 140 kN and 160 kN, respectively, but the tiny cracks did not extend until cracks were observed at the wall base when the lateral forces were increased to 360 kN for SCWA specimens. For SCWB specimens, concrete failure of the wall could not be observed because the concrete was covered by the steel faceplates and steel diaphragm. Specimen SCWB-1 was in an elastic deformation mode and the steel plates and steel diaphragms were in plane with loads less than 180 kN. A small crack of length 60 mm occurred at the junction of the wall side and wall base at 200 KN, as shown in Figure 9(c), and was concentrated and extended along the corner to the bottom with the continual loading. No unusual phenomenon was observed for specimen SCWB-2 with loads less than 340 kN. Small cracks with a length of 100 mm occurred at the junction of the wall base and wall when the load was 360 kN, as shown in Figure 9(d). The crack at the wall base extended to the bottom of the wall base with continual loading, as shown in Figure 9(e).

As observed in the experiment, the cracks at the wall side occurred in the loading range from 100 kN to 120 kN, with the exception that the wall sides of specimens SCWB-1 and SCWB-2 could not be observed. When the loading was up to 25–40% of peak load, the specimen was at the onset of concrete fracture.

Figure 9. Flexural cracking of the infill concrete for the specimens

2.1.2. Yielding and local buckling of steel faceplate

The steel faceplate of SCWA-1 yielded and buckled locally at loadings of 320 kN and 360 kN, respectively, and the distances between the concrete and the steel were about 1 mm and 3 mm, respectively, as shown in Figures 10(a) and 10(b). For specimen SCWA-2, the steel faceplate yielded at a load of 440 kN, at a distance of 2 mm from the top of the wall base, as shown in Figure 10(c), after which displacement-control was used. The deformation speed rapidly increased and outside buckling of the steel faceplate extended from the corner to the middle when the displacement was 16 mm, as shown in Figure 10(d). Pulling out of the steel diaphragms at the two sides was observed in the tension area at loadings of ±340 kN in specimen SCWB-1, and it moved 4 mm from its original position, as shown in Figure 10(e). The displacement of the wall increased after running at that loading. The steel faceplate yielded at a load of 400 kN, after which displacement-control was used, as shown in Figure 10(f). The welding between the steel faceplate and the steel diaphragm was damaged when the displacement was 24 mm (the loading was about 420 kN), in which the tearing length was about 50 mm, as shown in Figure 10(g). The deformation sharply increased, the steel at the bottom was avulsed, and the concrete at the junction of the wall base and wall side was damaged when the loading was continued, as shown in Figure 10(h). The steel diaphragm of SCWB-2 was pulled out when the load was 440 kN, and the length was about 5 mm, as shown in Figur 10(i). The steel faceplate yielded and extended to the middle at a load of 480 kN, as shown in Figure 10(j). The welding between the faceplate and the steel diaphragm was damaged at a displacement of 28 mm (520 kN), and the damaged length was about 60 mm, as shown in Figure 10(k).

2.1.3. Crushing and spalling of the infill concrete and final failure of SC wall piers

Crushing and spalling of the infill concrete is shown in Figure 11. After the yielding and local buckling of the two steel faceplates, the infill concretes at the two sides of the bottom in the specimens SCWA were crushed. The crushing and spalling of the infill concrete occurred in specimens SCWA-1 and SCWA-2 at a lateral force of 500 kN and at a displacement of 16 mm, respectively, as shown in Figures 11(a) and 11(b).

Large displacement, crushing and spalling of the concrete at the toe of the wall, and faceplate buckling were observed at the termination of the tests for the SCWA and SCWB specimens. The over failure modes of specimens SCWA and SCWB are shown in Figure 12.The peak loads were 520 kN, 570 kN, 500 kN, and 650 kN, respectively.

a) Steel yield (SCWA-1)

b) Steel buckling (SCWA-1)

c) Steel yield (SCWA-2)

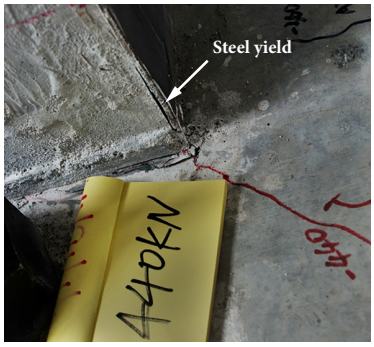

d) Steel buckling to the middle (SCWA-2)

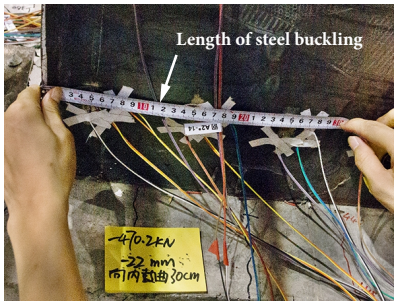

e) Steel diaphragm being pulled out (SCWB-1)

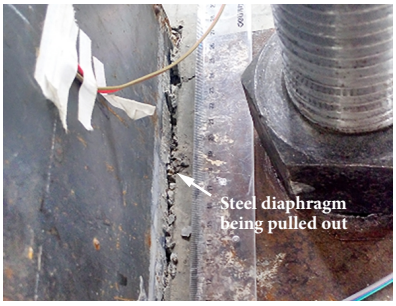

f) Steel faceplate yield (SCWB-1)

g) Buckling and welding damage (SCWB-1)

h) Steel avulsion (SCWB-1)

i) Pulled out of steel diaphragm (SCWB-2)

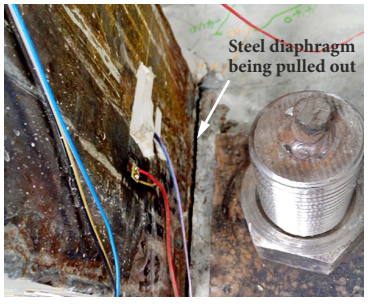

j) Steel buckling (480 kN) (SCWB-2)

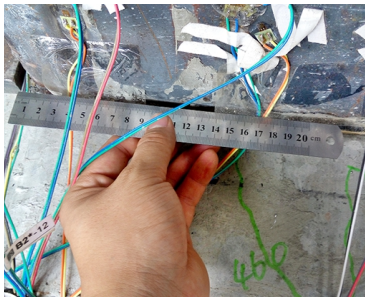

k) Welding damage (SCWB-2

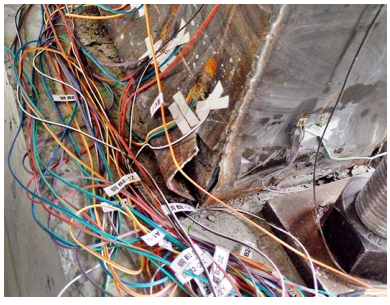

Figure 10. Yielding and local buckling of steel faceplate for the specimens

2.2. Load-displacement cyclic response

The lateral load-displacement relationships for specimens SCWA through SCWB are presented in Figure 13. SCWA-1 showed slip deformation and an asymmetric load- displacement relationship, as in Figure 13(a), because the anchoring between the wall base and the foundation trench was not strong enough. SCWA-1 was tested first, and when we found the problem, we improved the anchoring for other specimens, so other specimens did not slip. Ductility in the specimen SCWA-1 decreased in the negative direction due to the wall slip. The hysteretic loop curve showed obvious pinching phenomenon. As a result, the bearing capacity and ductility of specimens were reduced.

a) Crushing and spalling of the infill concrete (SCWA-1)

b) Crushing and spalling of the infill concrete (SCWA-2)

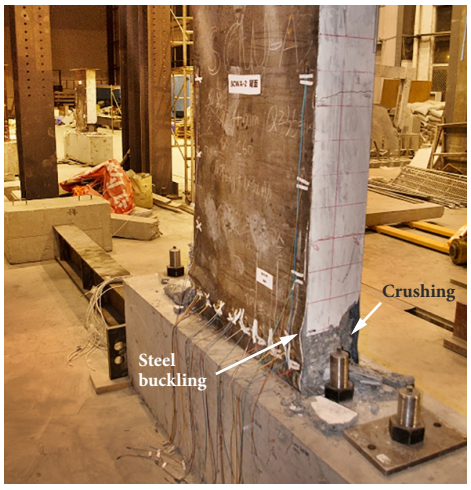

Figure 11. Crushing and spalling of the infill concrete

a) Over failure modes of specimens SCWA-1

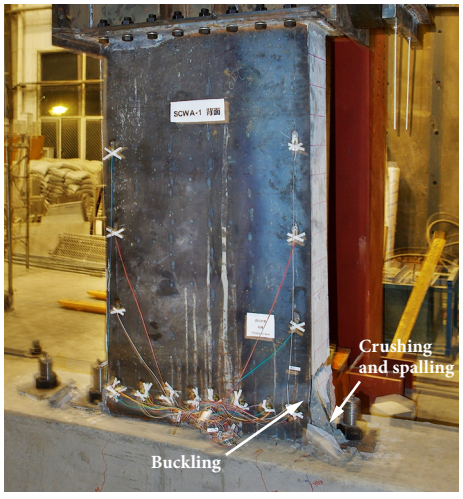

b) Over failure modes of specimens SCWA-2

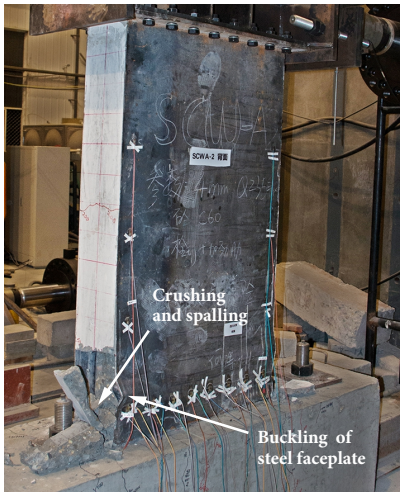

c) Over failure modes of specimens SCWB-1

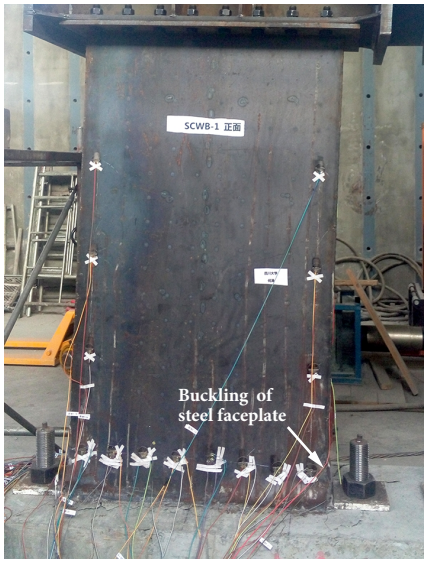

d) Over failure modes of specimens SCWB-2

Figure 12. Over failure modes of specimens SCWA and SCWB

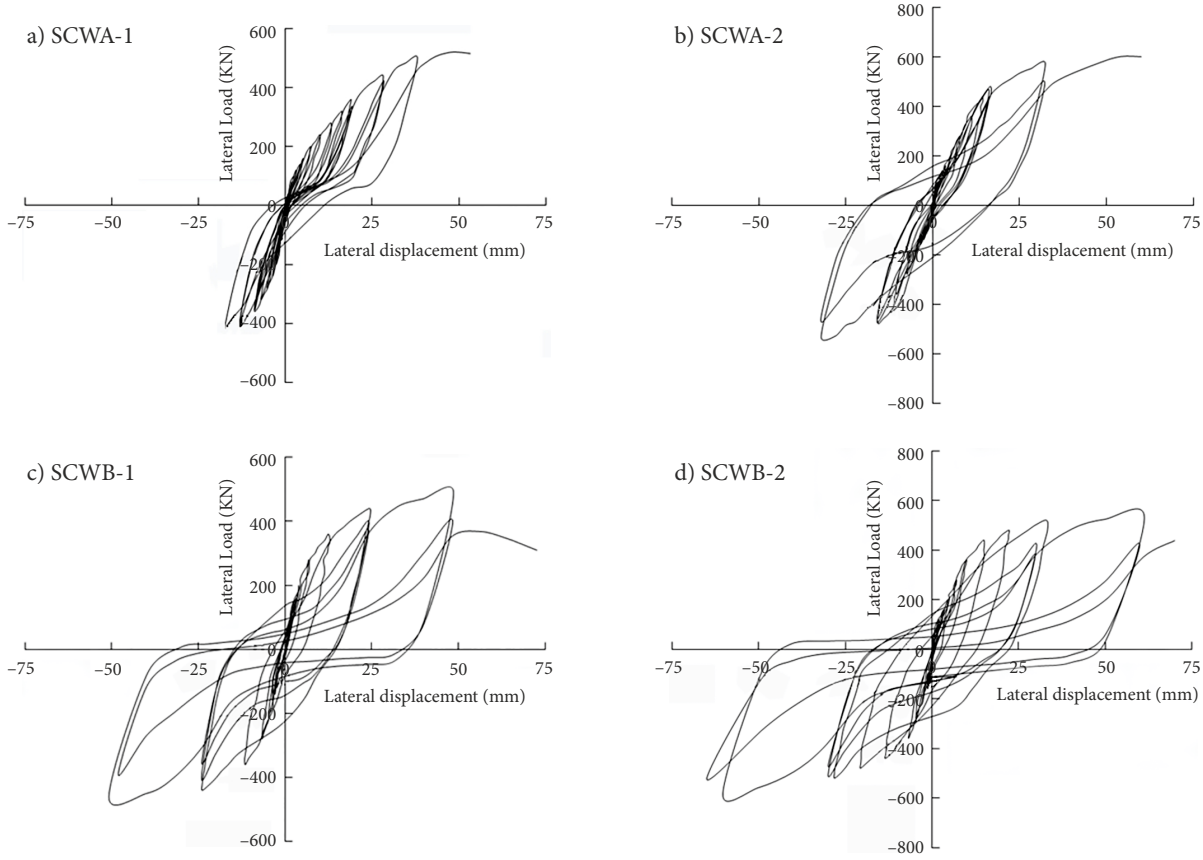

Figure 13. Lateral load-displacement relationships of specimens

In the SC wall, the bottom structure connected with the wall has a great influence on the performance of the SC wall. So in the actual design process, the connection between the SC wall and the bottom structure should be guaranteed. A less pinched hysteresis, greater peak load, and higher energy-dissipating capacity were observed in the load-displacement relationships of specimens SCWA-2 and SCWB-2, compared with specimens SCWA-1 and SCWB-1, respectively. This shows that the faceplate thickness has a significant effect on the seismic performance of SC wall piers. Specimen SCWB, as a chamber structure with steel diaphragms connecting the two faceplates, had a greater hysteresis area, stronger deformation, larger peak load, better ductility, and higher energy-dissipating capacity than SCWA. This shows that chamber structures have a better seismic performance.

2.3. Analysis of energy-dissipating capacity

An equivalent viscous damping coefficient h_e (Roy & Craig, 1981) is used as an index to evaluate the energy-dissipating capacity of SC wall piers, which is defined as follows:

$$h_e = \frac{1}{2\pi}\frac{S_{ABCA}}{S_{OBE} + S_{OFD}}, \quad (1)$$

where S_{ABCA} refers to the hysteresis area and energy-dissipating capacity, and $S_{OBE} + S_{OFD}$ represents the elastic energy of a specimen, as shown in Figure 14(a).

Figures 14(b) and 14(c) present the energy-dissipating capacity and h_e curves for specimens SCWA and SCWB. The energy-dissipating capacity and h_e both increase with continual loading, until the load is up to the peak load. The energy-dissipating capacity and h_e curves then degrade because of the damage in the specimens after the peak load. The energy-dissipating capacity and h_e of specimens SCWB are greater than those of specimens SCWA, which indicates that SCWB, as a chamber structure by setting steel diaphragms to connect the two faceplates, had a higher energy-dissipating capacity.

2.4. Analysis of stiffness degradation

The equivalent stiffness K is used as the specimen stiffness of the peak load at each cyclic loading, as defined in Eqn (2). Figure 15 shows the equivalent stiffness versus displacement relationship of SCWA and SCWB specimens. Table 3 summarizes the relevant results for these specimens including the cracking stiffness (K_{cr}), yielding stiffness (K_y), and peak load stiffness (K_p). When the steel faceplate starts to yield, the specimen enters the yielding stage. The displacement at this time is selected as yield displacement, which is used to calculate the yielding stiffness. The progression of the stiffness degradation in the four SCWA and SCWB specimens was sequentially (1) a sharp, high-speed degradation from the initial stiffness to the onset of concrete fracture, (2) a medium speed degradation

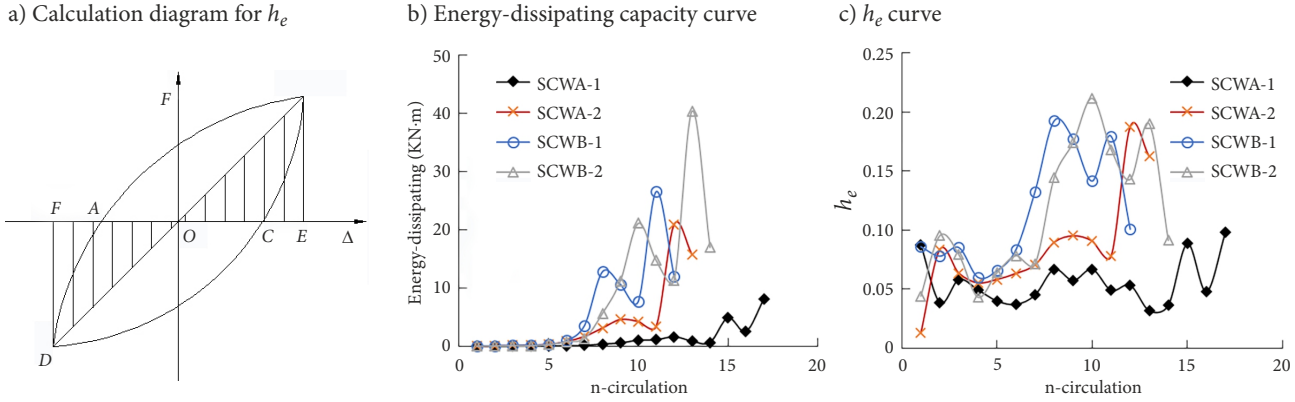

Figure 14. Energy-dissipating capacity and h_e curves

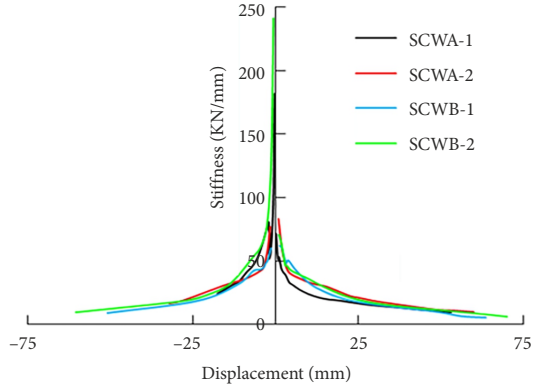

Figure 15. Stiffness versus displacement curve

from the onset of concrete fracture to the onset of steel faceplate yielding, and stiffness degradation percentages of 61% and 71% for SCWA-1 and SCWA-2, respectively, (3) a slow-speed degradation from the onset of steel yielding to peak load, with stiffness degradation percentages of 46%, 58%, 54%, and 55% for SCWA-1, SCWA-2, SCWB-1, and SCWB-2, respectively, and (4) stable stiffness from the peak load to the specimen failure.

The stiffness of SCWA-1 is greater than that of SCWA-2 in the area of negative displacement because SCWA-1 was not strengthened sufficiently at the foundation and subsequently rotated. The initial stiffness of SCWA-2 and SCWB-2 was generally greater than that of SCWA-1 and SCWB-2, and the initial stiffness of SCWB was also substantially larger than that of SCWA. Both a higher steel faceplate thickness and a chamber structure can increase the initial stiffness of a specimen.

$$K_i = \frac{|F_i|}{|\Delta_i|}. \tag{2}$$

Table 3. Stiffness details

Specimens	K_{cr}	K_y	K_p
SCWA-1	51.81	19.70	10.45
SCWA-2	100.00	28.70	11.09
SCWB-1		22.73	10.07
SCWB-2		21.58	9.68

3. Numerical modeling and parametric analysis

A numerical study was undertaken using the finite element program ABAQUS. The following sections present the material constitutive model, element type, modeling assumptions, analysis results, and parametric analysis.

3.1. Material constitutive model

The constitutive model of the concrete used was a concrete damage plasticity model, which can address material damage, opening and closing of cracks, and loss of strength and stiffness under reversed cyclic lateral loading. Stress-strain curves and damage-plasticity strain curves of concrete in tensile and compression are required in ABAQUS. However, the damage evolution parameter of concrete is not defined in ABAQUS, and it is obtained according to the Code for Design of Concrete Structures (GB 50010-2010, 2010). In this paper, the stress-strain curve of concrete under uniaxial tensile loading is defined as follows:

$$\sigma = (1 - d_t) E_c \varepsilon; \tag{3}$$

$$d_t = \begin{cases} (1 - \rho_t [1.2 - 0.2x^5] & x \le 1 \\ 1 - \dfrac{\rho_t}{\alpha_t (x-1)^{1.7} + x} & x > 1 \end{cases}; \tag{4}$$

$$x = \frac{\varepsilon}{\varepsilon_{t,r}}; \tag{5}$$

$$\rho_t = \frac{f_{t,r}}{E_c \varepsilon_{t,r}}; \tag{6}$$

$$\varepsilon_{t,r} = f_{t,r}^{0.54} \times 65 \times 10^{-6}; \tag{7}$$

$$\alpha_t = 0.312 f_{t,r}^2, \tag{8}$$

where α_t denotes a parameter value at the degradation branch of the stress-strain curve of concrete in uniaxial tensile. $f_{t,r}$ and d_t refer to uniaxial tensile strength and damage evolution parameter of concrete in uniaxial tensile, respectively. $\varepsilon_{t,r}$ indicates peak tensile strain of concrete corresponding to $f_{t,r}$.

The stress-strain curve of concrete in uniaxial compression is described as follows:

$$\sigma = (1 - d_c) E_c \varepsilon; \tag{9}$$

$$d_c = \begin{cases} 1-\dfrac{\rho_c n}{n-1+x^n} & x \le 1 \\ 1-\dfrac{\rho_c}{\alpha_c (x-1)^2 + x} & x > 1 \end{cases}; \tag{10}$$

$$\rho_c = \frac{f_{c,r}}{E_c \varepsilon_{c,r}}; \tag{11}$$

$$n = \frac{E_c \varepsilon_{c,r}}{E_c \varepsilon_{c,r} - f_{c,r}}; \tag{12}$$

$$x = \frac{\varepsilon}{\varepsilon_{c,r}}; \tag{13}$$

$$\varepsilon_{t,r} = (700 + 172\sqrt{f_c}) \times 10^{-6}; \tag{14}$$

$$\alpha_c = 0.157 f_c^{0.785} - 0.905; \tag{15}$$

$$\frac{\varepsilon_{cu}}{\varepsilon_{c,r}} = \frac{1}{2\alpha_c}(1 + 2\alpha_c + \sqrt{1+4\alpha_c}), \tag{16}$$

where α_c denotes a parameter value at the degradation branch of the stress-strain curve of concrete in uniaxial compression. $f_{c,r}$ and d_c refer to uniaxial compression strength of concrete and damage evolution parameter of concrete in uniaxial compression, respectively. $\varepsilon_{c,r}$ indicates peak tensile strain of concrete corresponding to $f_{c,r}$.

$$W_0^e = \frac{\sigma^2}{2E_0}; \tag{17}$$

$$W_d^e = \frac{\overline{\sigma^2}}{2E_d}; \tag{18}$$

$$\overline{\sigma} = (1-d)\sigma; \tag{19}$$

$$E_d = E_0 (1-d)^2; \tag{20}$$

$$\sigma = E_0 (1-d)^2 \varepsilon, \tag{21}$$

where $W_0^e = \dfrac{\sigma^2}{2E_0}$ and $W_d^e = \dfrac{\overline{\sigma^2}}{2E_d}$ represent elastic complementary energies in no damage material and in equivalent damage material, respectively. Substitute Eqns (3) to (16) into (21), and the damage evolution parameters in uniaxial tensile and compression can be defined in Eqns (22) and (23), respectively.

$$d_t' = \begin{cases} 1-\sqrt{\rho_t [1.2 - 0.2x^5}} & x \le 1 \\ 1-\sqrt{\dfrac{\rho_t}{\alpha_t (x-1)^{1.7} + x}} & x > 1 \end{cases}; \tag{22}$$

$$d_c' = \begin{cases} 1-\sqrt{\dfrac{\rho_c n}{n-1+x^n}} & x \le 1 \\ 1-\sqrt{\dfrac{\rho_c}{\alpha_c (x-1)^2 + x}} & x > 1 \end{cases}. \tag{23}$$

The relevant parameters of C60 concrete used in this finite element analysis are as follows: elastic modulus, Poisson's ratio, expansion angle, eccentricity ratio, uniaxial compressive strength, uniaxial tensile strength, the ratio of biaxial compressive strength f_{b0} to uniaxial compressive strength f_{c0}, curve shape parameter, and viscosity parameter are 3.3×10^4 MPa, 0.2, 35°, 0.1,30.25 MPa, 2.51 MPa, 1.16, 0.66667, and 0.0005, respectively. The stress-strain curves of C60 concrete under the compression and tension, and the damage factor parameters of the tensile and compression are shown in Table 4.

Table 4. Constitutive relation of plastic damage model of concrete

Compressive stress (MPa)	Plastic strain	Compression damage	Tension stress (MPa)	Cracking strain	Tensile damage
33.96	0.0000	0.0660	3.00	0.0000	0.1584
37.16	0.0002	0.0954	2.61	0.0001	0.2841
39.36	0.0003	0.1293	1.90	0.0001	0.4526
40.59	0.0005	0.1664	1.45	0.0002	0.5637
40.97	0.0007	0.2055	1.25	0.0002	0.6162
38.44	0.0011	0.2976	1.10	0.0002	0.6572
30.81	0.0018	0.4377	0.93	0.0003	0.7042
24.05	0.0026	0.5467	0.81	0.0003	0.7394
20.59	0.0030	0.6021	0.74	0.0003	0.7583
17.85	0.0035	0.6468	0.69	0.0004	0.7745
14.74	0.0041	0.6991	0.62	0.0004	0.7949
12.46	0.0047	0.7386	0.57	0.0004	0.8116
11.27	0.0051	0.7599	0.54	0.0005	0.8213
10.27	0.0055	0.7781	0.51	0.0005	0.8299
9.05	0.0060	0.8009	0.48	0.0005	0.8413
8.08	0.0066	0.8195	0.45	0.0006	0.8511
7.53	0.0070	0.8301	0.43	0.0006	0.8570
7.05	0.0073	0.8396	0.42	0.0006	0.8624
6.44	0.0079	0.8520	0.40	0.0006	0.8697
5.91	0.0084	0.8627	0.38	0.0007	0.8762
5.61	0.0088	0.8690	0.37	0.0007	0.8802
5.33	0.0092	0.8748	0.35	0.0007	0.8838
4.97	0.0097	0.8825	0.34	0.0008	0.8889
4.65	0.0103	0.8894	0.33	0.0008	0.8936
4.46	0.0106	0.8935	0.32	0.0008	0.8964
4.28	0.0110	0.8974	0.31	0.0008	0.8991
4.04	0.0115	0.9026	0.30	0.0009	0.9029
3.82	0.0121	0.9074	0.29	0.0009	0.9064
3.69	0.0124	0.9103	0.28	0.0009	0.9086
3.57	0.0128	0.9131	0.28	0.0010	0.9106
3.40	0.0133	0.9169	0.27	0.0010	0.9136
3.25	0.0139	0.9204	0.26	0.0010	0.9163
3.15	0.0142	0.9226	0.26	0.0011	0.9180
3.06	0.0146	0.9247	0.25	0.0011	0.9196
2.94	0.0151	0.9275	0.25	0.0011	0.9219
2.82	0.0156	0.9302	0.24	0.0011	0.9241
2.75	0.0160	0.9319			
2.68	0.0163	0.9335			
2.58	0.0169	0.9358			
2.49	0.0174	0.9379			
2.44	0.0178	0.9392			

An ideal double linear model was used as the steel constitutive model. Plasticity strain, elasticity modulus, Poisson's ratio, yield strength and ultimate strength of steel are 0.15, 2.06×10^5 MPa, 0.3, 255 MPa and 395 MPa, respectively.

3.2. Model details

Penalty friction was used to consider the contact between the steel faceplates and the infilled concrete. Other parts are considered to be perfectly connected with each other. A T3D2 truss element was used to represent the rebar in the wall base. An eight-node solid element C3D8R was used to model the steel faceplates, studs, infilled concrete, stiffening ribs, steel webs, and tie robs. The model is shown in Figure 16. A reference node was set 10 mm above the top of the center of the specimen and was coupled with the specimen. The load and displacement were applied on the reference node to prevent large deformation and singularity of the specimen. An area load of 0.8 N/mm was applied on the top of specimen, which was equal to a vertical load 150 kN. The bottom of the foundation was fixed.

3.3. Comparison of numerical results with experimental results

The ABAQUS-predicted and measured cyclic backbone curves for specimens are presented in Figure 17. The numerical results have a good match with the experimental results for specimen SCWA, including a similar development trend and peak load. The initial stiffnesses of the numerical models are always larger than those of the experiments because ideal boundary conditions were assumed, which are stronger than the actual test conditions. Another reason may be that the bottom of the foundation was not completely fixed and the foundation rotated in the test.

Figure 18 shows the failure modes and stress nephogram for the numerical and experimental results. The failure form for the specimens SCWA-2 and SCWB-2 in the experimental and the numerical results are shown in Figures 18(a), 18(b), 18(c) and 18(d), respectively. The Figures 18(b) and 18(d) mainly show the deformation shape in ABAQUS after loading. the stress nephogram of steel and concrete for the specimens SCWA-2 and SCWB-2 are shown in Figures 18(e), 18(f), 18(g), and 18(h), respectively. The maximum stresses of the steel in Figures 18(f) and 18(h) are 365 MPa and 395 MPa, respectively. The yield strength and ultimate strength of steel are 255 MPa and 395 MPa, respectively. The stresses in the wall from the bottom to the middle are larger than the yield strength 255 MPa, and the stresses at the corner of the bottom reach the ultimate strength 395 MPa. The maximum stresses occur at the corner of the bottom of the SC wall. The wall from the bottom to the middle yields and the corner of the bottom is damaged. The yielding extends from the edge of the bottom to the inside. These are consistent with the experiment results, as shown in Figures 18(a) and 18(c). The maximum stresses of the concrete in Figures 18(e) and 18(g) are 41.8 MPa and 28.28 MPa at the corner of the bottom, and they are all compressive stresses. The uniaxial compressive strength and uniaxial tensile strength of the concrete are 30.25 MPa and 2.51 MPa, respectively. In the specimen SCWA-2, the stresses of the corner of the concrete bottom are larger than the uniaxial compressive strength 30.25 MPa and the concrete is crushed and damaged, which is in good agreement with the results of the experiment, as shown in Figure 18(a). For the specimen SCWB-2, the maximum stress 28.28 MPa is less than the uniaxial compressive strength 30.25 MPa, and the concrete is not damaged.

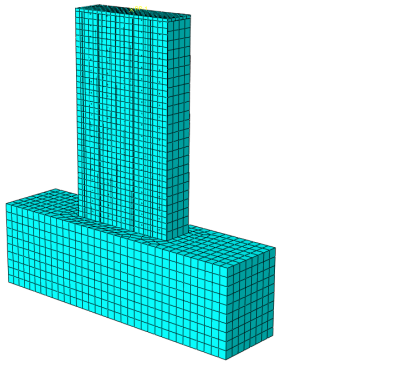

Figure 16. Mesh of specimen model

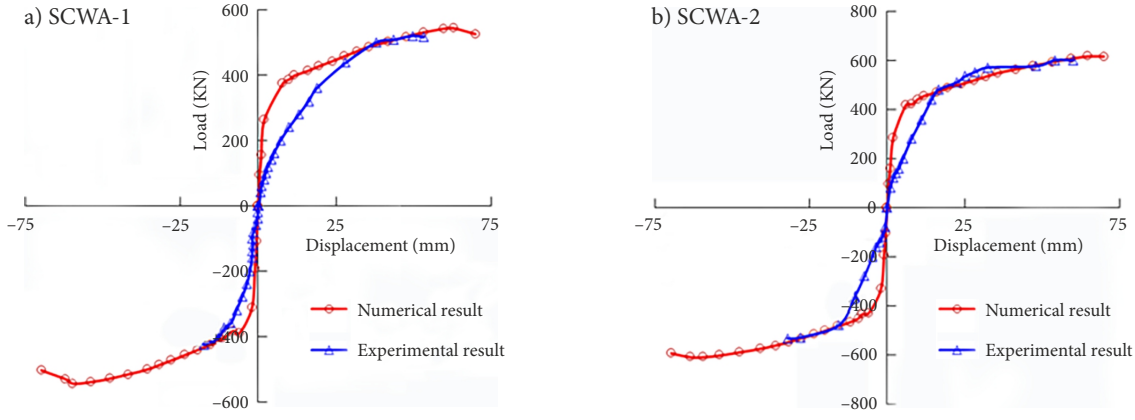

Figure 17. Cyclic backbone curves

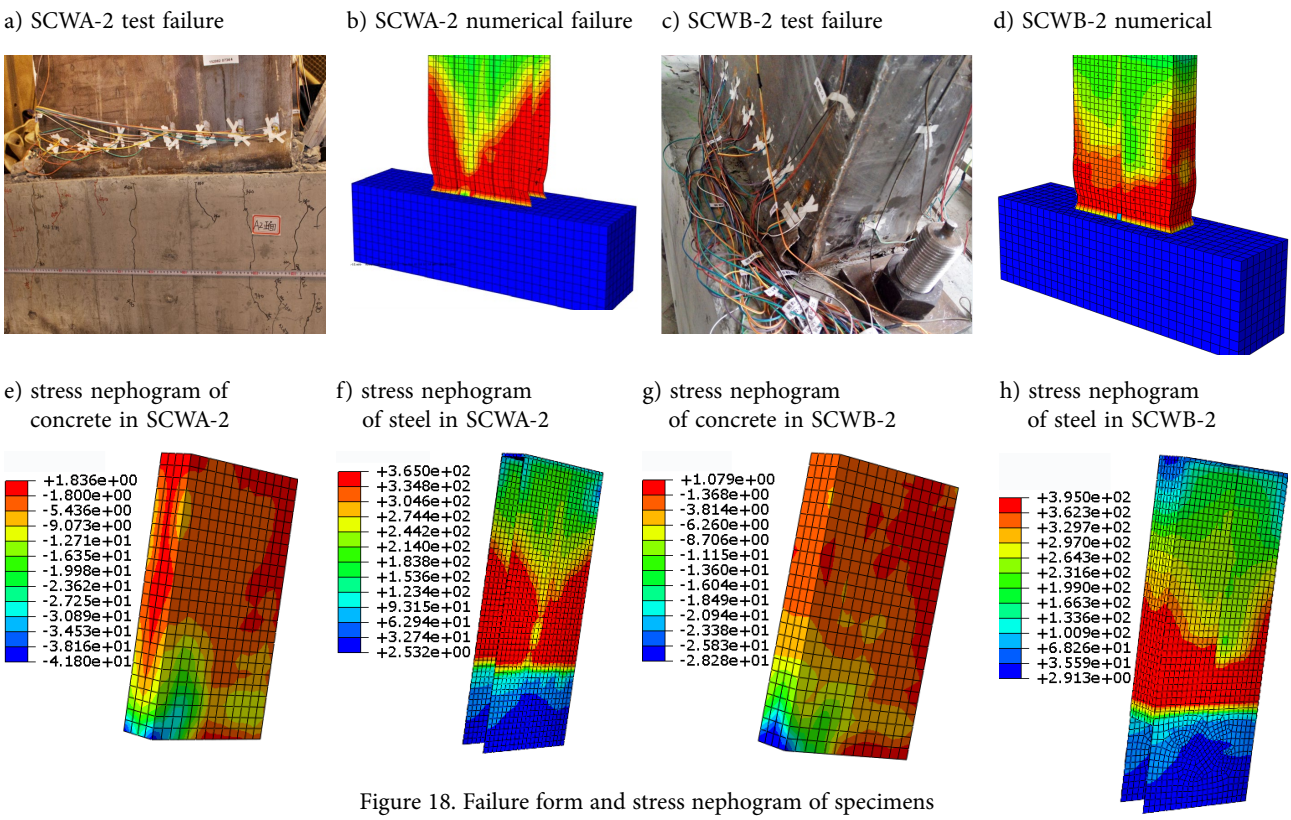

Figure 18. Failure form and stress nephogram of specimens

The compressive stress of the concrete is less than the uniaxial tensile strength 2.51 MPa. Analysis of the ABAQUS model predicts damage of the steel faceplates and steel webs above the wall base, which was also observed in the experiment, as shown in Figures 18(a) an 18(c). The deformation of the steel in ABAQUS is in good agreement with the experiments, as shown in Figures 18(b) and 18(d). The damage of the SC walls, buckling of the steel faceplates and steel webs are captured quite well by the ABAQUS models, and the numerical models can be used to further parametric analysis.

3.4. Parametric analysis results

Parametric analysis was conducted to further investigate the effect of different parameters on the seismic response of SC walls. The parameters include stiffening rib, steel web amount, material strength, shear-span ratio, and axial compression ratio.

3.4.1. Stiffening rib and steel web amount

Specimen SCWB was designed as a chamber structure and had a higher peak load and displacement than SCWA according to the experimental results. However, the loads at the onset of concrete cracking were close to each other. In order to study the parameters which affect the concrete cracking, another two numerical models, SCWB-1-SR and SCWB-1-SW, based on the design of SCWB-1, as shown in Figures 19(b) and 19(c), were conducted to analyze the effects of stiffening ribs and steel webs on the response of the SC walls. Figure 21 and Table 5 provides the backbone curves, key loads and displacements.

SCWB-1-SW with four steel webs did not have significantly better seismic performance than that of SCWB-1. The peak load in SCWB-1-SW was only 3.7% more than that in SCWB-1. The increase of the steel web amount had little effect on the SC wall performance.

A stiffening rib was included in SCWB-1-SR. The peak load and displacement for SCWB-1-SR was significantly improved by 33% and 84%, respectively, which indicates that the ductility and energy-dissipating capacity are both increased. The percentages of the differences for the load and displacement of concrete cracking were 86% and 76%. The load at concrete cracking is very important for the safety of nuclear power plants and can be increased by putting stiffening ribs in the SC walls.

3.4.2. Material strength

Backbone curves for different material strengths are presented in Figure 20. The backbone curves of SCWA and SCWB with varying concrete strength are almost the same when the concrete strength is greater than 30 N/mm^2. The concrete strength has a small effect on the concrete crack load. The steel strength can significantly increase the yielding and peak loads, however it has little effect on the load and the displacement of the concrete crack, yielding and the peak displacements. The yield and peak loads for SCWA-7-Q345, compared with SCWA-1-Q235, are increased by 39% and 14%, respectively, and 29% and 16% for SCWB-7-Q345, compared with SCWB-1-Q235, respectively. Increasing the steel faceplate thickness can be a method to improve the bearing capacity of SC walls.

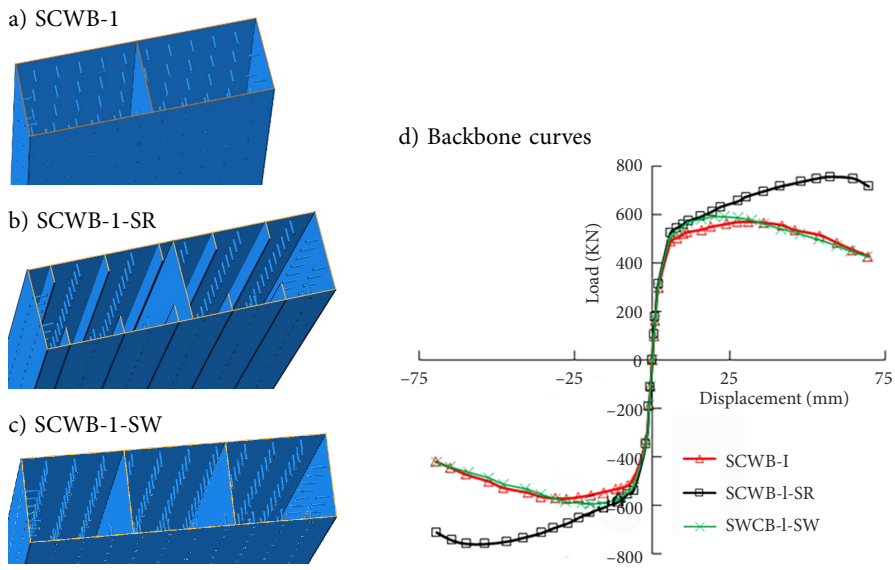

Figure 19. Parametric results for stiffening rib and steel web amount

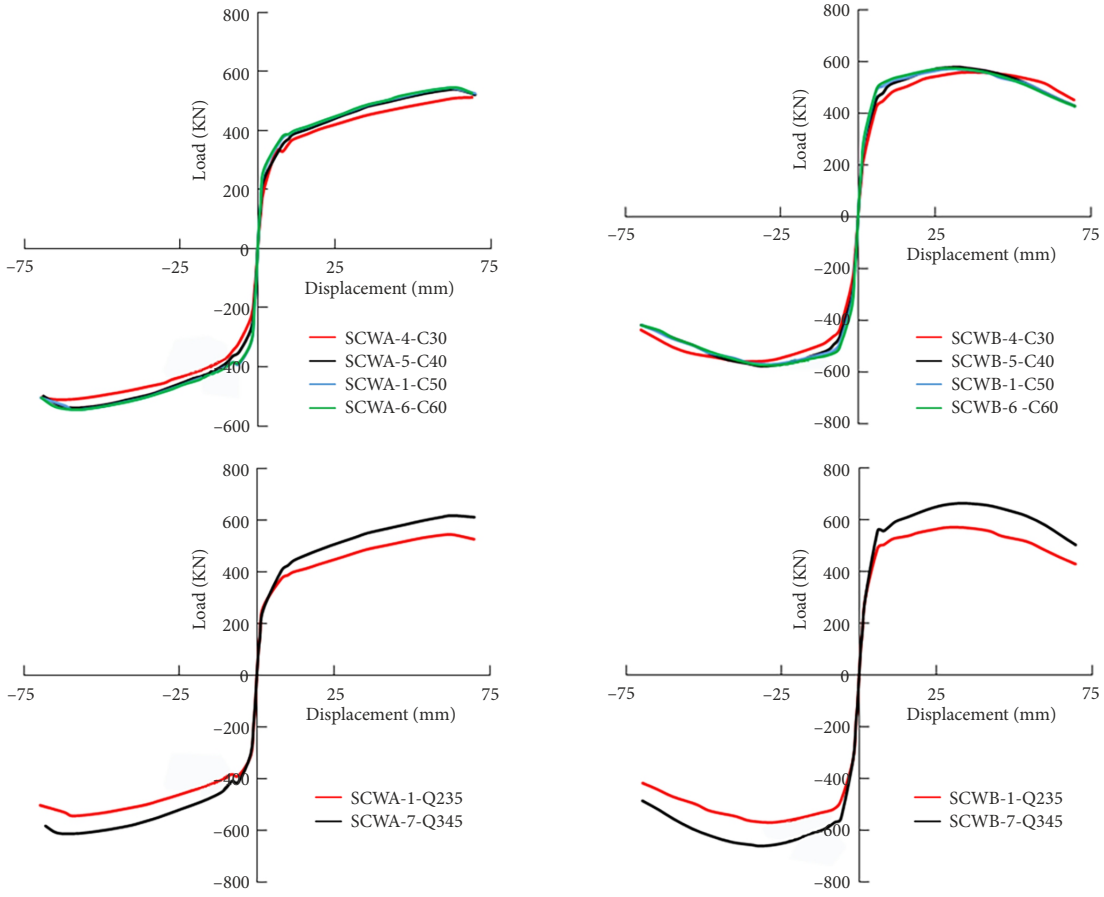

Figure 20. Backbone curves for models of different material strength

Table 5. Key loads and displacements

Models	Structure difference	Concrete crack		Yielding		Peak	
		Load (kN)	Displacement (mm)	Load (kN)	Displacement (mm)	Load (kN)	Displacement (mm)
SCWB-1	No stiffening rib	79	0.29	316	1.8	570	31
SCWB-1-SW	Increasing steel web	74	0.26	325	1.8	591	23
SCWB-1-SR	Increasing stiffening rib	147	0.51	341	1.89	755	57

3.4.3. Shear-span ratio and axial compression ratio

Figure 21 shows the backbone curves of models with different shear-span ratios. The smaller the shear-span ratio is, the bigger the crack and yielding loads, however, there are smaller cracks and yield displacements. In this condition, the ductility and energy-dissipating capacity decrease and shear failure occurs. This is due to the low cyclic reversed loading, in which the specimen is under horizontal shear load and bending moment, and the shear-span directly affects the bending moment. The smaller the shear-span ratio is, the closer it is to shear failure damage.

The backbone curves of Figure 22 provide information that a large axial compression ratio can improve the load and displacement where the concrete cracks, the yield load, and peak load, however, such increases are less than 10%. The displacement at peak loading is larger in the model with greater axial compression ratio, and increasing the axial compression ratio can improve ductility and energy-dissipating capacity.

Summary and conclusions

Four large-size steel–plate concrete composite walls were tested, with design parameters including steel faceplate thickness and internal structural elements (stiffening rib, steel diaphragm), to investigate the earthquake resistance of SC walls subjected to reversed cyclic lateral loading. A new chamber structure, using steel diaphragms to connect the two faceplates and to divide the wall into two parts, is proposed in this paper. The key outcomes and conclusions of the present study are summarized as follows:

1. SC wall piers with a chamber structure and steel diaphragms connecting the two faceplates, have less hysteresis pinching, greater hysteresis area, stronger deformation, larger peak load, better ductility, and higher energy-dissipating capacity.
2. For SC walls with a chamber structure, increasing the steel webs has little effect on the seismic response. Stiffening ribs can significantly improve the peak load and displacement, ductility, energy-dissipating capacity, and concrete crack load and displacement but it has little effect on the yield load.
3. Increasing the steel strength can improve the bearing capacity but not the ductility and energy-dissipating capacity. Reducing the shear-span ratio leads to higher crack and yield loads but lower crack and yield displacements. The higher axial compression ratio can improve ductility and energy-dissipating capacity. Both a higher steel faceplate thickness and chamber structure can increase the initial stiffness of specimen.

According to the experimental results and the parameter analysis by the ABAQUS finite element model, three suggestions for SC wall design are put forward for reference in practical engineering design:

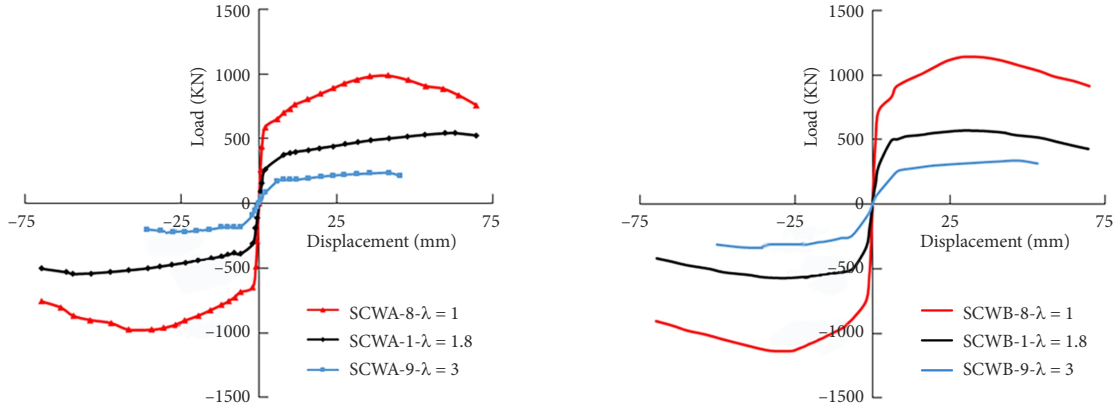

Figure 21. Backbone curves for different shear-span ratio

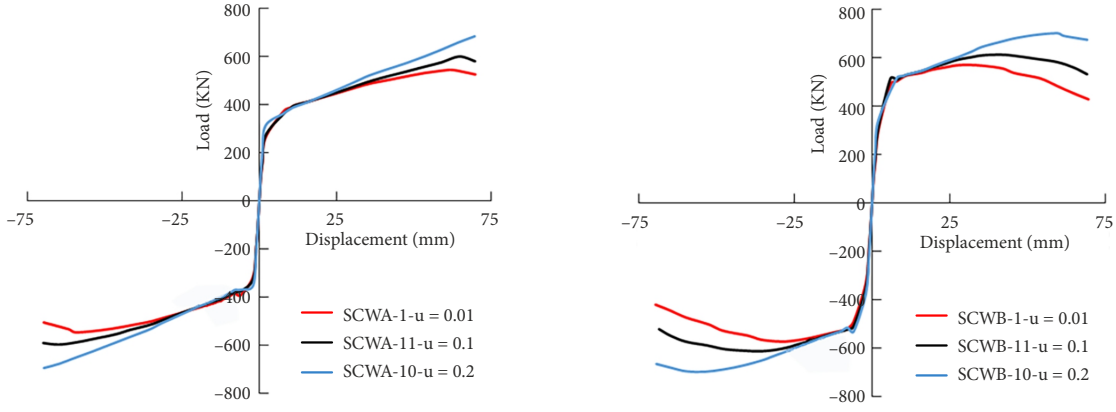

Figure 22. Backbone curves for different axial compression ratio

1. The strength of concrete has no significant influence on the seismic performance of SC walls, while the thickness of the steel faceplate has a great influence on its seismic performance. When the seismic capacity of SC walls cannot meet the requirements, the thickness of the steel faceplate can be increased to improve the yield load and peak load of the wall.
2. When increasing the thickness of the steel faceplate cannot meet the bearing capacity requirements, the chamber structure with steel diaphragms joining the two faceplates to each other and dividing the SC wall piers into several parts can be considered. The crack resistance of concrete can be improved by increasing the number of stiffening ribs, and the performance of other walls can also be improved.
3. When SC walls are directly connected with the foundations or other structures, the performance of foundations or other structures has a great effect on SC walls. Firstly, it is necessary to ensure that the foundations or other structures have sufficient bearing capacity. For the foundations, the steel faceplates are adequate when enough deeply inserted into to the foundations so as to prevent the bearing capacity of the wall from being reduced due to the destruction of the foundation or the pulling out of the steel faceplates.

Acknowledgements

The authors gratefully acknowledge the financial support of the Subproject of the National Natural Science Foundation of China (Grant No.: 51508357) and the science and technology innovation cooperation plan among Hong Kong, Macao and Taiwan, the international scientific and technological innovation cooperation of Sichuan province, China (Grant No.: 2019YFH0120). The authors are also grateful to the laboratory technicians for their assistance in making the specimens.

Funding

This work was supported by the <National Natural Science Foundation of China> under Grant [number 51508357] and the international scientific and technological innovation cooperation of Sichuan province, China (number: 2019YFH0120).

Author contributions

Qi Ge and Feng Xiong conceived the study and were responsible for the design of the experiment and development of the data analysis. Tao He was responsible for implementation of the experiments. Ning Zhou was responsible for data collection and analysis. Yang Lu was responsible for parametric analysis. Qi Ge wrote the first draft of the article.

References

ACI 349 Committee. (2006). *Code requirements for nuclear safety-related concrete structures* (*ACI 349-06*) *and commentary*. Farmington Hills, MI.

Ali, A., Kim, D., & Cho, S. G. (2013). Modeling of nonlinear cyclic load behavior of Ishaped composite steel-concrete shear walls of nuclear power plants. *Nuclear Engineering and Technology*, *45*(1), 89–98. https://doi.org/10.5516/NET.09.2011.055

American Concrete Institute (ACI). (2014). *ACI 318 – Building code requirements for structural concrete and commentary*. Farmington Hills, MI.

Anwar, H. K. M., & Wright, H. D. (2004). Experimental and theoretical behaviour of composite walling under in-plane shear. *Journal of Constructional Steel Research*, *60*, 59–83. https://doi.org/10.1016/j.jcsr.2003.08.004

Board of KEPIC Policy Structural Committee. (2010). *KEPIC SNG – SNG steel plate concrete structures*. Seoul, Korea.

Booth, P. N., Varma, A. H., Malushte, S. R., & Johnson, W. H. (2007). Response of modular composite walls to combined thermal and mechanical load. In *19th International Conference on Structural Mechanics in Reactor Technology* (*SMiRT19*). International Association for Structural Mechanics in Reactor Technology (IASMiRT). Toronto, Canada.

Booth, P. N., Varma, A. H., Sener, K., & Malushte, S. (2015). Flexural behavior and design of steel-plate composite (SC) walls for accident thermal loading. *Nuclear Engineering and Design*, *295*, 817–828. https://doi.org/10.1016/j.nucengdes.2015.07.036

Braverman, J., Morante, R., & Hofmayer, C. (1997). *Assessment of modular construction for safety related structures at advanced nuclear power plants* (NUREG/CR-6486). U.S. Nuclear Regulatory Commission. Washington DC. https://doi.org/10.2172/464149

Bruhl, J., Varma, A. H., & Johnson, W. (2015a). Design of composite SC walls to prevent perforation from missile impact. *International Journal of Impact Engineering*, *75*, 75–87. https://doi.org/10.1016/j.ijimpeng.2014.07.015

Bruhl, J., Varma, A. H., & Joo, M. M. (2015b). Static resistance function for steel-plate composite (SC) walls subjected to impactive loading. *Nuclear Engineering and Design*, *295*, 843–859. https://doi.org/10.1016/j.nucengdes.2015.07.037

Chaudhary, S., Ali, A., Kim, D., & Cho, S. G. (2011). Seismic analysis of steel concrete composite walls of nuclear power plant structures. In *21th International Conference on Structural Mechanics in Reactor Technology* (*SMiRT21*). International Association for Structural Mechanics in Reactor Technology (IASMiRT). New Delhi, India.

Choi, B. J., & Han, H. S. (2009). An experiment on compressive profile of the unstiffened steel plate-concrete structures under compression loading. *Steel and Composite Structures*, *9*(6), 519–534. https://doi.org/10.12989/scs.2009.9.6.519

Choi, B. J., Kim, W. K., Kim, W. B., & Kang, C. K. (2013). Compressive performance with variation of yield strength and width-thickness ratio for steel plate-concrete wall structures. *Steel and Composite Structures*, *14*(5), 473–491. https://doi.org/10.12989/scs.2013.14.5.473

DCD. (2011). *Design control document for the AP1000*. Washington, DC, USA: U.S. Nuclear Regulatory Commission. http://www.nrc.gov/reactors/new-reactors/design-cert/ap1000.html

DCD. (2012). *Design control document for the US-APWR*. Washington, DC, USA: U.S. Nuclear Regulatory Commission. http://www.nrc.gov/reactors/new-reactors/design-cert/apwr.html

Emori, K. (2002). Compressive and shear strength of concrete filled steel box wall. *International Journal of Steel Structures*, *2*(1), 29–40.

Eom, T. S., Park, H. G., Lee, C. H., Kim, J. H., & Chang, I. H. (2009). Behavior of double skin composite wall subjected to in-plane cyclic loading. *Journal of Structural Engineering*, *135*(10), 1239–1249. https://doi.org/10.1061/(ASCE)ST.1943-541X.0000057

Epackachi, S. (2014). *Analytical, numerical, and experimental studies on steel-concrete composite walls* (PhD Dissertation). Department of Civil, Structural and Environmental Engineering, University at Buffalo. NY, USA.

Epackachi, S., Nguyen, N. H., Kurt, E. G., Whittaker, A. S., & Varma, A. H. (2013). An experimental study of the in-plane response of steel-concrete composite walls. In *22nd International Conference on Structural Mechanics in Reactor Technology* (*SMiRT 22*). San Francisco, CA, USA.

Epackachi, S., Nguyen, N. H., Kurt, E. G., Whittaker, A. S., & Varma, A. H. (2015a). In-plane seismic behavior of rectangular steel-plate composite wall piers. *Journal of Structural Engineering*, *141*(7), 401–417. https://doi.org/10.1061/(ASCE)ST.1943-541X.0001148

Epackachi, S., Whittaker, A. S., & Huang, Y. N. (2015b). Analytical modeling of rectangular SC wall panels. *Journal of Constructional Steel Research*, *105*, 49–59. https://doi.org/10.1016/j.jcsr.2014.10.016

Epackachi, S., Whittaker, A. S., Varma, A. H., & Kurt, E. G. (2015c). Finite element modeling of steel-plate concrete composite wall piers. *Engineering Structures*, *100*, 369–384. https://doi.org/10.1016/j.engstruct.2015.06.023

Fukumoto, T., Kato, B., Sato, K., Toyama, K., Kobayashi, M., Emori, K, Ishii K., & Sakamoto. M. (1987). *Concrete filled steel bearing walls*. Zurich: International Association for Bridge and Structural Engineering.

GB 50010-2010. (2010). *Code for design of concrete structures*. Beijing, China.

Hong, S. G., Kim, W., Lee, K. J., Hong, N. K., & Lee, D. H. (2010). Out-of-plane shear strength of steel-plate-reinforced concrete walls dependent on bond behavior. *Journal of Disaster Research*, *5*(4), 385–394. https://doi.org/10.20965/jdr.2010.p0385

Huang, Z. Y., & Liew, J. Y. R. (2016). Numerical studies of steel-concrete-steel sandwich walls with J-hook connectors subjected to axial loads. *Steel and Composite Structures*, *21*(3), 461–477. https://doi.org/10.12989/scs.2016.21.3.461

Japanese Electric Association Nuclear Standards Committee. (2009). *JEAC 4618 – Technical code for seismic design of steel plate reinforced concrete structures: buildings and structures*. Tokyo, Japan.

Ji, X. D., Jiang, F. M., & Qian, J. R. (2013). Seismic behavior of steel tube–double steel plate–concrete composite walls: Experimental tests. *Journal of Constructional Steel Research*, *86*, 17–30. https://doi.org/10.1016/j.jcsr.2013.03.011

Ju, X. C., & Zeng, Z. B. (2015). Study on uplift performance of stud connector in steel-concrete composite structures. *Steel and Composite Structures*, *18*(5), 1279–1290. https://doi.org/10.12989/scs.2015.18.5.1279

Kim, W. B., & Choi, B. J. (2011). Shear strength of connections between open and closed steel-concrete composite sandwich structures. *Steel and Composite Structures*, *11*(2), 168–181. https://doi.org/10.12989/scs.2011.11.2.169

Kim, W., Lee, S. J., Jung, R. Y., & Kim, M. (2009, August). Damping values for seismic design of nuclear power plant SC structures. In *21th International Conference on Structural Mechanics in Reactor Technology* (*SMiRT20*). Espoo, Finland.

Kurt, E. G., Varma, A. H., Booth, P. N., & Whittaker, A. (2016). In-plane behavior and design of rectangular SC wall piers without boundary elements. *Journal of Structural Engineering*, *142*(6), 04016026. https://doi.org/10.1061/(ASCE)ST.1943-541X.0001481

Kurt, E. G., Varma, A. H., Booth, P., & Whittaker, A. S. (2013). SC walls piers and basemat connections: Numerical investigation of behavior and design. In *22nd International Conference on Structural Mechanics in Reactor Technology* (*SMiRT 22*). San Francisco, CA, USA.

Link, R. A., & Elwi, A. E. (1995). Composite concrete-steel plate walls: Analysis and behavior. *Journal of Structural Engineering*, *121*(2), 260–271. https://doi.org/10.1061/(ASCE)0733-9445(1995)121:2(260)

Nguyen, N. H., & Whittaker, A. S. (2017). Numerical modelling of steel-plate concrete composite shear walls. *Engineering Structures*, *150*, 1–11. https://doi.org/10.1016/j.engstruct.2017.06.030

Oduyemi, T. O. S., & Wright, H. D. (1989). An experimental investigation into the behaviour of double-skin sandwich beams. *Journal of Constructional Steel Research*, *14*, 197–220. https://doi.org/10.1016/0143-974X(89)90073-4

Ozaki, M., Akita, S., Oosuga, H., Nakayama, T., & Adachi, N. (2004). Study on steel plate reinforced concrete panels subjected to cyclic in-plane shear. *Nuclear Engineering and Design*, *228*, 225–244. https://doi.org/10.1016/j.nucengdes.2003.06.010

Remennikov, A. M., Kong, S. Y., & Uy, B. (2013). The response of axially restrained noncomposite steel–concrete–steel sandwich panels due to large impact loading. *Engineering Structures*, *49*, 806–818. https://doi.org/10.1016/j.engstruct.2012.11.014

Roy, R., & Craig, J. (1981). *Structural dynamics*. Wiley.

Schlaseman, C. (2004). *Application of advanced construction technologies to new nuclear power plants* (MPR-2610, Revision 2). Washington, DC, USA. http://pbadupws.nrc.gov/docs/ML0931/ML093160836.pdf

Sener, K. C., & Varma, A. H. (2014). Steel-plate composite walls: experimental database and design for out-of-plane shear. *Journal of Constructional Steel Research*, *100*, 197–210. https://doi.org/10.1016/j.jcsr.2014.04.014

Sener, K., Varma, A. H., & Seo, J. (2016). Experimental and numerical investigations of the shear behavior of steel-plate composite (SC) beams without shear reinforcement. *Engineering Structures*, *127*, 495–509. https://doi.org/10.1016/j.engstruct.2016.08.053

Sener, K., Varma, A. H., Booth, P. N., & Fujimoto, R. (2015). Seismic behavior of a containment internal structure consisting of composite SC walls. *Nuclear Engineering and Design*, *295*, 804–816. https://doi.org/10.1016/j.nucengdes.2015.07.038

Sener, K., Varma, A. H., Malushte, S. R., & Coogler, K. (2013). Experimental database of SC composite specimens tested under out-of-plane shear loading. In *22nd International Conference on Structural Mechanics in Reactor Technology* (*SMiRT22*). International Association for Structural Mechanics in Reactor Technology (IASMiRT). San Francisco, California, USA.

Seo, J., Varma, A. H., Sener, K., & Ayhan, D. (2016). Steel-plate composite (SC) walls: In-plane shear behavior, database, and design. *Journal of Constructional Steel Research*, *119*, 202–215. https://doi.org/10.1016/j.jcsr.2015.12.013

Sohel, K. M. A., & Liew, J. Y. R. (2014). Behavior of steel–concrete–steel sandwich slabs subject to impact load. *Journal of Constructional Steel Research*, *100*, 163–175. https://doi.org/10.1016/j.jcsr.2014.04.018

Takeuchi, M., Narikawa, M., Matsuo, I., Hara, K., & Usami, S. (1998). Study on a concrete filled structure for nuclear power plants. *Nuclear Engineering and Design*, *179*(2), 209–223. https://doi.org/10.1016/S0029-5493(97)00282-3

Usami, S., Akiyama, H., Narikawa, M., Hara, K., Takeuchi, M., & Sasaki, N. (1995). Study on a concrete filled steel structures for nuclear power plants (part 2). Comprehensive loading tests on wall members. In *13th International Conference on Structural Mechanics in Reactor Technology* (*SMiRT 13*). Porto Alegre, Brazil.

Varma, A. H., & Sener, K. C. (2013). Misubishi Heavy Industries. Lateral load behavior of a containment internal structure consisting of composite SC walls. In *22nd International Conference on Structural Mechanics in Reactor Technology* (*SMiRT 22*). San Francisco, CA, USA.

Varma, A. H., Malushte, S. R., Sener, K. C., & Booth, P. N. (2009). Analysis and design of modular composite walls for combined thermal and mechanical loading. In *20th International Conference on Structural Mechanics in Reactor Technology* (*SMiRT19*). International Association for Structural Mechanics in Reactor Technology (IASMiRT). Espoo, Finland. https://doi.org/10.1061/41031(341)103

Varma, A. H., Malushte, S. R., Sener, K., Booth, P. N., & Coogler, K. (2011a). Steel-plate composite (SC) walls: Analysis and design including thermal effects. In *21th International Conference on Structural Mechanics in Reactor Technology* (*SMiRT21*). International Association for Structural Mechanics in Reactor Technology (IASMiRT). New Delhi, India.

Varma, A. H., Malushte, S., Sener, C., & Lai, Z. (2014). Steel-plate composite (SC) walls for safety related nuclear facilities: Design for in-plane force and out-of-plane moments. *Nuclear Engineering and Design*, *269*, 240–249. https://doi.org/10.1016/j.nucengdes.2013.09.019

Varma, A. H., Sener, K. C., Zhang, K., Coogler, K., & Malushte, S. R. (2011b). Out-of-plane shear behavior of SC composite structures. In *21st International Conference on Structural Mechanics in Reactor Technology* (*SMiRT 21*). New Delhi, India.

Wright, H. (1998). The axial load behaviour of composite walling. *Journal of Constructional Steel Research*, *45*(3), 353–375. https://doi.org/10.1016/S0143-974X(97)00030-8

Zhang, K., Varma, A. H., Malushte, S., & Gallocher, S. (2014). Effects of shear connectors on the local buckling and composite action in steel concrete composite walls. *Nuclear Engineering and Design*, *269*, 231–239. https://doi.org/10.1016/j.nucengdes.2013.08.035

Zhao, W., & Guo, Q. (2018). Experimental study on impact and post-impact behavior of steel-concrete composite panels. *Thin-Walled Structures*, *130*, 405–413. https://doi.org/10.1016/j.tws.2018.06.012